Glacier mass changes on the Tibetan Plateau 2003 – 2009 derived from ICESat laser altimetry measurements (Supplementary Material)

N. Neckel[1], J. Kropáček[1,2], T. Bolch[2,3], and V. Hochschild[1]

[1]Institute of Geography, University of Tübingen, Rümelinstr. 19-23, 72070 Tübingen, Germany

[2]Institute for Cartography, Dresden University of Technology, Helmholzstr. 10, 01062 Dresden, Germany

[3]Department of Geography, University of Zurich, Winterthurer Str. 190, 8057 Zürich, Switzerland

E-mail: Niklas.Neckel@uni-tuebingen.de

Additional information on data

In this study we chose the GLA 14 product over the GLA 06 product, which is frequently used to derive ice sheet elevations, because of the mountainous topography and crevassed glacier surfaces in our study area (Kääb, 2008). The main difference between the GLA 06 and GLA 14 data product is the higher number of Gaussian fits applied to the return signal of the GLA 14 data. The GLAS elevation data, originally referenced to the Topex/Poseidon ellipsoid, were adjusted to the WGS84 ellipsoid following Bhang et al. (2007) and corrected for EGM96-geoid variations obtained from the GLA 14 dataset. The recently announced range determination error of ±6 cm in the ICESat data can be neglected as the GLA 14 product seems to be not affected by this error (Zwally, 2013). The approximate June laser periods (2C, 3C, 3F) were excluded from the analysis as they only include the first three years of ICESat's lifetime and could therefore bias the results. Also laser period 2F was excluded from the analysis due to a failure of the laser in this period.

In this study we use version 3 of the SRTM-C DEM (90 m grid spacing) which is available to the public via the U.S. Geological Survey (USGS) at *dds.cr.usgs.gov/srtm/version2_1/SRTM3/*. Compared to version 4 of the DEM no timely inconsistent data patches and interpolation artifacts are present in version 3 and no horizontal misalignment between version 3 and the ICESat data is found which is in agreement with Kääb et al. (2012, their supplementary information). However, data gaps are present in version 3 of the DEM but are located in off-glacier areas in our study region. The vertical reference of the SRTM-C DEM is the EGM96-geoid.

Additional information on methods

For the separation into accumulation and ablation areas in each sub-region, Equilibrium Line Altitude (ELA) values were selected from the literature (Table S 1). The data describing the ELA on the TP are sparse and heterogeneous both in terms of the acquisition method and date taken. Some authors used field measurements (Ageta et al., 1989; Pu et al., 2008; Fujita and Nuimura, 2011) while others reconstructed the ELA using a model (Ageta and Kadota, 1992; Benn and Lehmkuhl, 2000; Caidong and Sorteberg, 2010). Due to the sparse spatial data coverage of published ELA values, additional information was derived from recent Landsat imagery acquired in September/October 2010 (Thematic Mapper, Level 1, acquisition). The snowline was manually selected for several glaciers with different angles of inclination and slope in the relevant sub-regions. The mean of the snowline elevations was used as an approximate ELA in the respective sub-regions. For comparison we calculated the median glacier elevation in each sub-region which gives a rough approximation of the ELA if the glaciers are in equilibrium (Raper and Braithwaite, 2009). In order to test the sensitivity to a changing ELA we added ±150 m to our ELA estimates, which revealed a mean difference of ±30% for the derived ΔH trends.

Supplementary Table S 1. Equilibrium line altitude (ELA) values for the eight sub-regions. Also shown glacier median elevation in each sub-region, year of ELA estimate and data source.

sub-region	median (m)	ELA (m)	year	source
A	5,944	5,930	1987	Ageta et al. (1989)
B	5,867	5,835	2010	Landsat estimate
C	5,372	5,300	2010	Landsat estimate
D	5,635	5,740	2002	Pu et al. (2008)
E	5,756	5,770	2005	Caidong and Sorteberg (2010)
F	5,757	5,600	2005	Fujita and Nuimura (2011)
G	5,512	5,500	2010	Landsat estimate
H	4,871	4,860	1989	Ageta and Kadota (1992)

It is known that ICESat measurements tend to get inaccurate on slopes >10° (e.g. Hilbert and Schmullius, 2012). We therefore tested the sensitivity of ΔH trends on slopes <10°, which revealed a mean difference of -0.04 m a^{-1} for the ΔH trends in all sub-regions with the highest deviation of -0.26 m a^{-1} in sub-region G where 50% of on-glacier ICESat footprints were excluded. Due to the large number of discarded ICESat measurements no slope threshold was applied for our final estimate.

Error computation

In order to test the representativeness of ICESat coverage we employed a bootstrapping analysis (e.g. Kääb et al., 2012). Here we included random ICESat footprints in 10% intervals and calculated ΔH trends after each iteration. After 200 iterations we calculated the standard deviation of trends which is shown in Figure S 2 (all acquisitions) and Figure S 7 (autumn acquisitions) and fitted a polynomial to the data. As at some point the standard deviation of trends reaches a stable value we included the polynomial value where 100% of the ICESat footprints are included in the analysis as an error for the uneven spatial data sampling in our error estimate. This value reaches from 0.09 m a^{-1} for sub-region B to 0.21 m a^{-1} for sub-region E. We also detected a temporal trend in the ICESat data which is shown in Figure S 4. However, as our bootstrapping analysis shows a stable value at ∼60% of included ICESat footprints we conclude that the temporal trend of decreasing ICESat measurements (-5.9±3.8% a^{-1}) and the differences of the area-elevation distribution (±15%, Figure S 1a) are covered by our error estimate. The overall error in surface elevation changes is given by

$$e_{trend} = \sqrt{\sigma_{trend}^2 + trend_{land}^2 + e_{bias}} \quad (1)$$

where σ_{trend} is the error from the bootstrapping analysis and $trend_{land}$ is the estimated off-glacier ΔH trend in each sub-region. The off-glacier trend was calculated in the same way as the on-glacier trend employing all off-glacier ICESat measurement in each sub-region. Following Gardner et al. (2013) we also included a systematic inter campaign bias of 0.06 m a^{-1} (e_{bias}). For the error estimate of the separate ΔH trends (i.e. in the accumulation area and the ablation area) we additionally included a ±30% ELA uncertainty.

For the error computation of mass balances we added an error of ±60 kg m^{-3} in ice density (Huss, 2013) and of ±20% in glacier area. For the latter we randomly selected 11 glaciers all of which are included in our analysis. The areas of these glaciers were digitized manually, based on the mentioned Landsat imagery (Thematic Mapper, Level 1, acquisition between 2003 and 2011). From the differences between the digitized glacier outlines and the CGI we estimated the error in glacier area.
In order to test the statistical significance (Z) of the derived ΔH trends we employed a Mann-Kendall trend test. If $|Z| \geq 1.96$ the estimated trend is assumed to be statistical significant at the 5% level.

ICESat footprint distribution

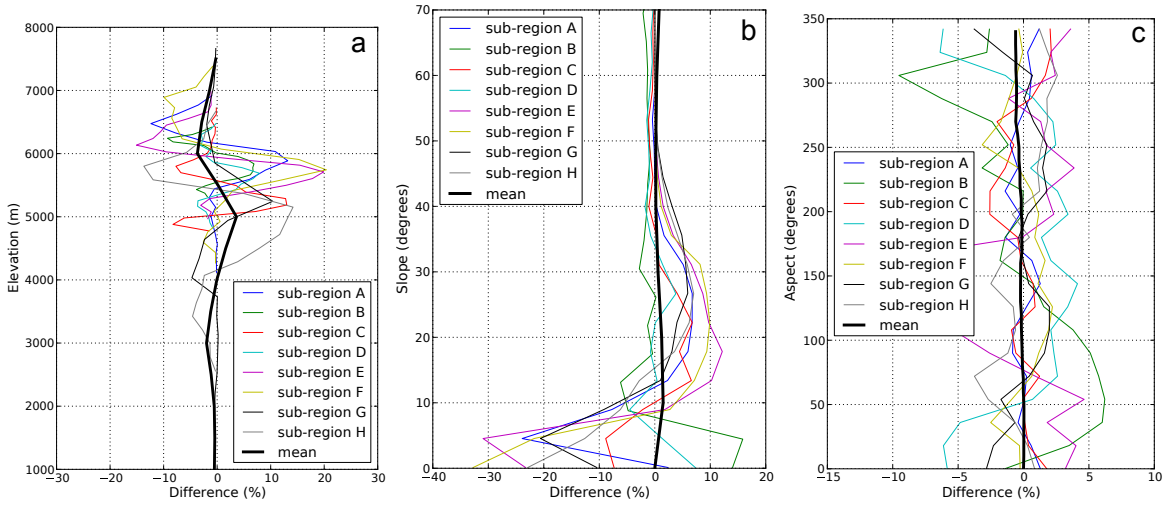

Supplementary Figure S 1. Difference between the area-elevation distribution and the ICESat elevation distribution for all glaciers in the eight sub-regions (**a**, after Bolch et al., 2013). In order to translate the ICESat footprint distribution to an area-elevation estimate we employed the 90 m grid posting of the SRTM-C DEM and the SRTM-C elevation at each ICESat footprint location. Difference between the glacier slope distribution and the ICESat slope distribution (**b**) and difference between the glacier aspect distribution and the ICESat aspect distribution (**c**).

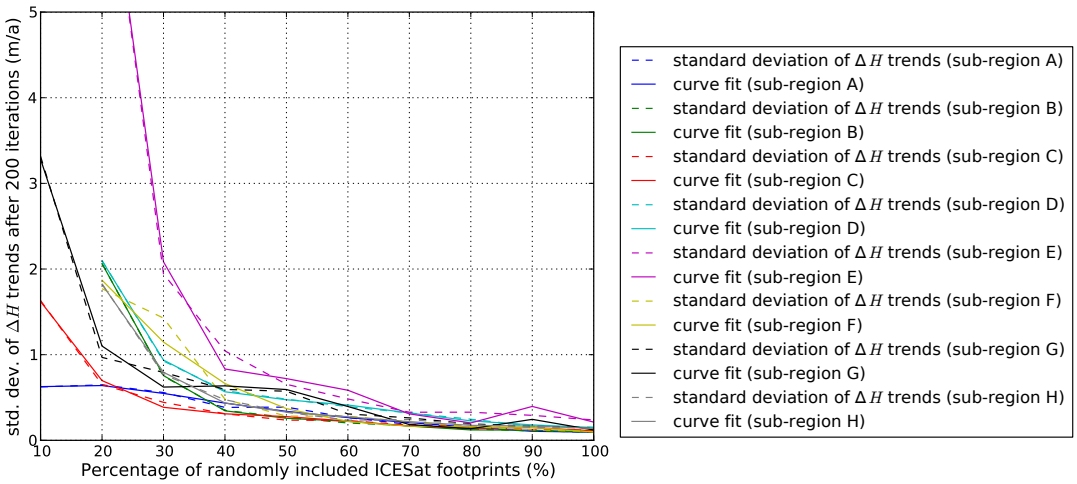

Supplementary Figure S 2. Standard deviation of ΔH trends from randomly selected 10% intervals of ICESat measurements after 200 iterations. The curves reach a stable value at ∼60% of included ICESat footprints, showing the representativeness of the ICESat data sample in each sub-region.

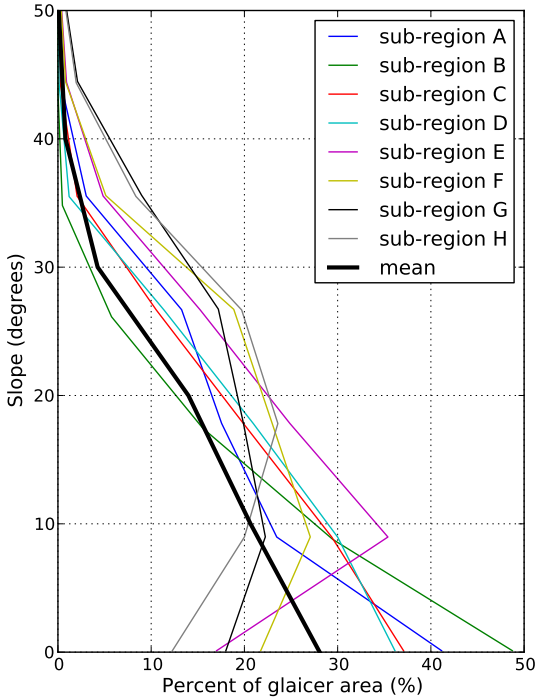

Supplementary Figure S 3. Glacier slope distribution for the eight sub-regions.

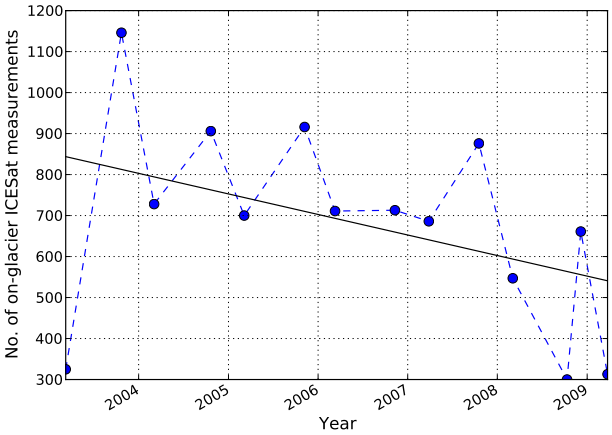

Supplementary Figure S 4. Temporal trend in the ICESat data sample. Blue dots represent the number of on-glacier ICESat measurements from each laser period (except for laser period 2C, 3C, 3F and 2F). The number of ICESat measurements is decreasing by -5.9±3.8% a^{-1} between 2003 and 2009.

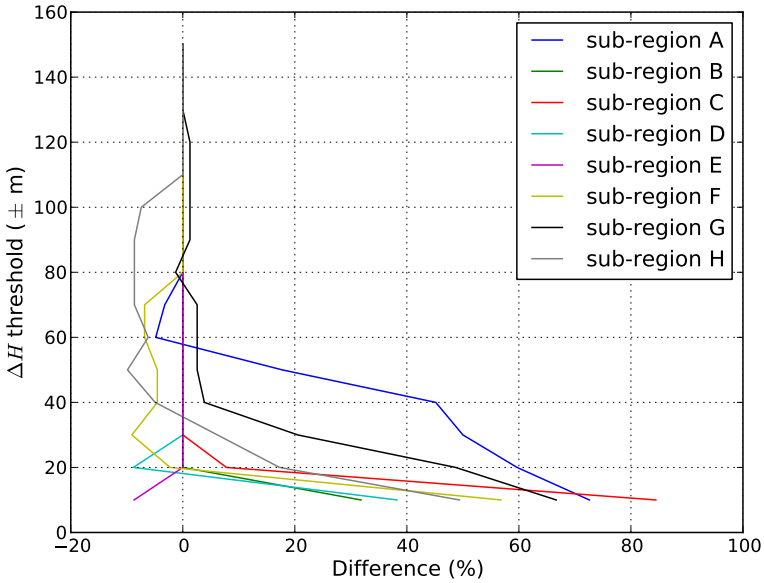

Supplementary Figure S 5. Difference of ΔH trends for a varying ΔH threshold in each sub-region. In order to select cloud-free ICESat footprints a ΔH threshold of ±150 m was applied to the data.

ICESat autumn measurements

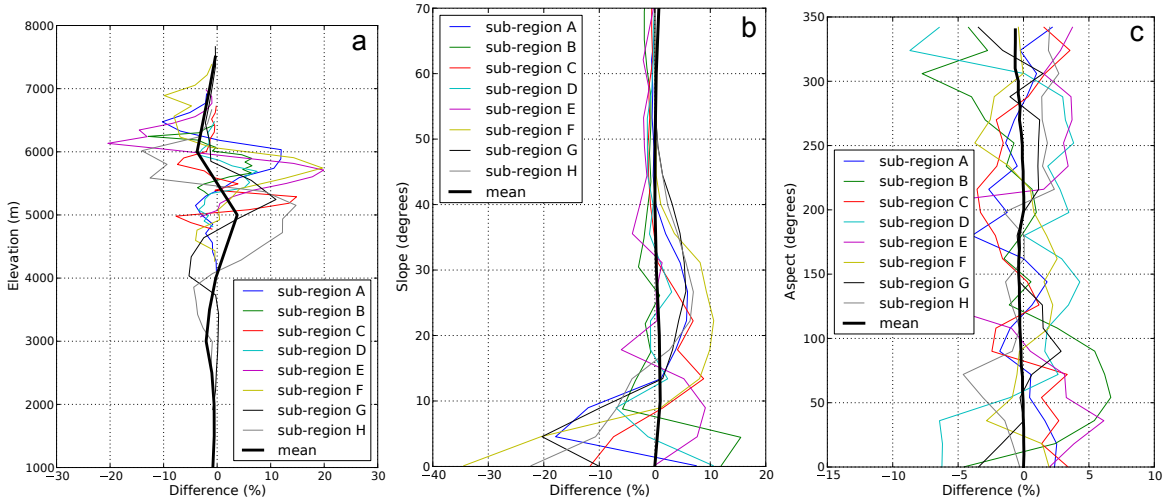

Supplementary Figure S 6. Same plot as Figure S 1 except that only autumn acquisitions are employed.

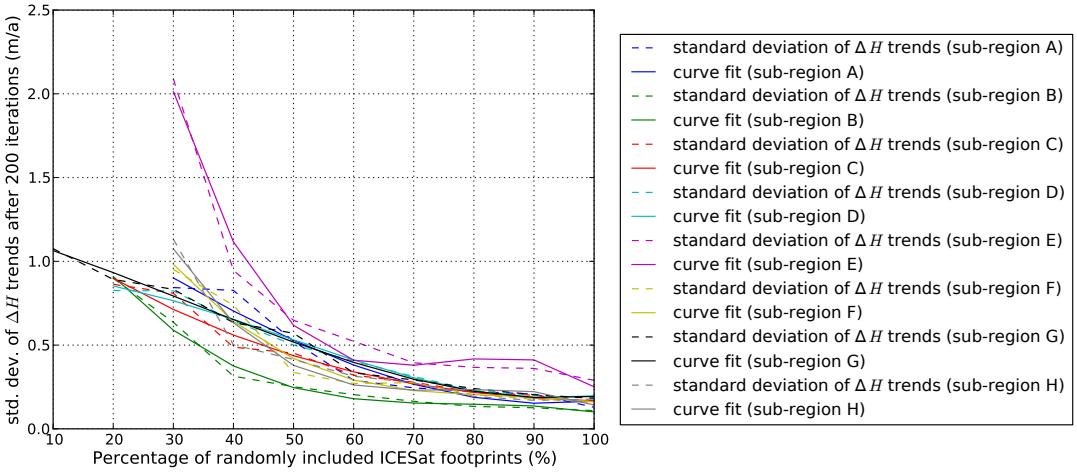

Supplementary Figure S 7. Same plot as Figure S 2 except that only autumn acquisitions are employed. A stable value is reached after including ∼90% of ICESat measurements.

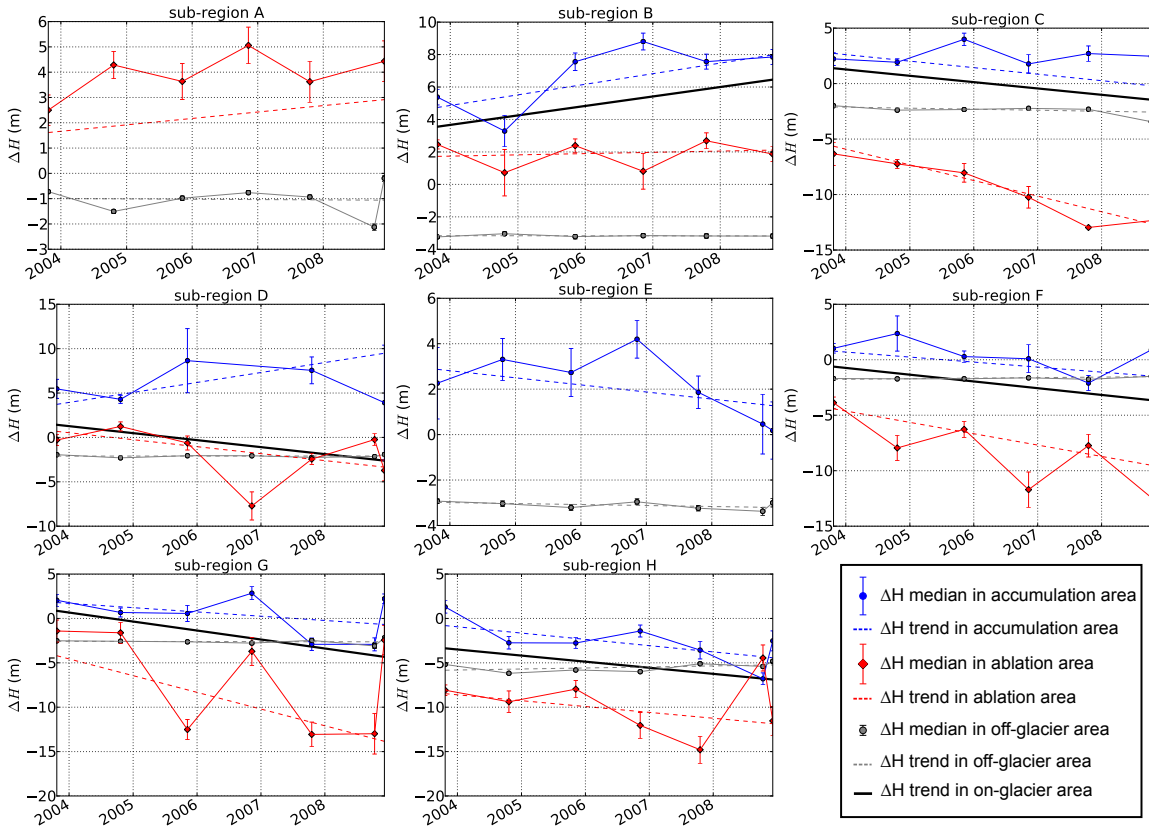

Supplementary Figure S 8. Estimated trends for selected geographic sub-regions solely based on autumn acquisitions. Geographic sub-regions are shown in Figure 1 in the manuscript. Trends were fitted through all ΔH values in on- and off-glacier areas. For on-glacier areas trends are shown separately for the accumulation and ablation areas as well as for the whole glacier area. For clarity reasons only the ΔH median of each laser period is shown. Year dates correspond to 1 January of each year.

Supplementary Table S 2. Regional trends of glacier elevation changes solely based on autumn acquisitions are shown next to the area weighted mass balance and total glacier area in each sub-region. Geographic location of sub-regions is shown in Figure 1 in the manuscript and trend lines are shown in Figure S 8. Statistical significant trends are illustrated as bold numbers.

Sub-region	ΔH trend (m a^{-1}) accumulation area	ΔH trend (m a^{-1}) ablation area	ΔH trend (m a^{-1}) on-glacier area	ΔH trend (m a^{-1}) off-glacier area	Mass balance (m w.e. a^{-1})	Total glacier area (km^2)
A	-	**+0.25±0.30**	+0.25±0.30[a]	-0.01±0.14	+0.21±0.26[a]	6,483
B	**+0.65±0.33**	+0.08±0.27	**+0.58±0.26**	-0.01±0.02	**+0.49±0.28**	464
C	-0.59±0.36	**-1.41±0.52**	-0.57±0.31	-0.09±0.11	-0.48±0.31	1,491
D	+1.12±0.46	**-0.79±0.39**	**-0.79±0.31**	+0.01±0.03	**-0.67±0.35**	1,859
E	-0.31±0.37	-	-0.31±0.37[b]	-0.12±0.03	-0.26±0.33[b]	1,056
F	**-0.45±0.33**	**-1.02±0.43**	**-0.61±0.30**	+0.05±0.02	**-0.52±0.31**	2,371
G	**-0.48±0.34**	**-1.88±0.64**	**-1.01±0.31**	-0.01±0.06	**-0.86±0.39**	6,632
H	**-0.71±0.37**	**-0.66±0.37**	**-0.69±0.31**	+0.12±0.10	**-0.59±0.33**	12,017

[a] data only available in ablation area.
[b] data only available in accumulation area.

References

Ageta, Y. and Kadota, T. (1992). Predictions of changes of glacier mass balance in the Nepal Himalaya and Tibetan Plateau: a case study of air temperature increase for three glaciers. *Annals of Glaciology*, 16:89–94.

Ageta, Y., Zhang, W., and Nakawo, M. (1989). Mass balance studies on Chongce Ice Cap in the West Kunlun Mountains. *Bulletin of Glacier Research*, 7:37–43.

Benn, D. I. and Lehmkuhl, F. (2000). Mass balance and equilibrium-line altitudes of glaciers in high-mountain environments. *Quaternary International*, 6566(0):15–29.

Bhang, K. J., Schwartz, F. W., and Braun, A. (2007). Verification of the Vertical Error in C-Band SRTM DEM Using ICESat and Landsat-7, Otter Tail County, MN. *IEEE Transactions on Geoscience and Remote Sensing*, 45(1):36–44.

Bolch, T., Sørensen, L. S., Simonsen, S. B., Mölg, N., Machguth, H., Rastner, P., and Paul, F. (2013). Mass loss of Greenland's glaciers and ice caps 2003-2008 revealed from ICESat laser altimetry data. *Geophysical Research Letters*, 40(5):875–881.

Caidong, C. and Sorteberg, A. (2010). Modelled mass balance of Xibu glacier, Tibetan Plateau: sensitivity to climate change. *Journal of Glaciology*, 56:235–248.

Fujita, K. and Nuimura, T. (2011). Spatially heterogeneous wastage of Himalayan glaciers. *Proceedings of the National Academy of Sciences*, 108:14011–14014.

Gardner, A. S., Moholdt, G., Cogley, J. G., Wouters, B., Arendt, A. A., Wahr, J., Berthier, E., Hock, R., Pfeffer, W. T., Kaser, G., Ligtenberg, S. R. M., Bolch, T., Sharp, M. J., Hagen, J. O., van den Broeke, M. R., and Paul, F. (2013). A Reconciled Estimate of Glacier Contributions to Sea Level Rise: 2003 to 2009. *Science*, 340(6134):852–857.

Hilbert, C. and Schmullius, C. (2012). Influence of Surface Topography on ICESat/GLAS Forest Height Estimation and Waveform Shape. *Remote Sensing*, 4(8):2210–2235.

Huss, M. (2013). Density assumptions for converting geodetic glacier volume change to mass change. *The Cryosphere*, 7(3):877–887.

Kääb, A. (2008). Glacier Volume Changes Using ASTER Satellite Stereo and ICESat GLAS Laser Altimetry. A Test Study on Edgeøya, Eastern Svalbard. *IEEE Transactions on Geoscience and Remote Sensing*, 46:2823–2830.

Kääb, A., Berthier, E., Nuth, C., Gardelle, J., and Arnaud, Y. (2012). Contrasting patterns of early twenty-first-century glacier mass change in the Himalayas. *Nature*, 488(7412):495–498.

Pu, J., Yao, T., Yang, M., Tian, L., Wang, N., Ageta, Y., and Fujita, K. (2008). Rapid decrease of mass balance observed in the Xiao (Lesser) Dongkemadi Glacier, in the central Tibetan Plateau. *Hydrological Processes*, 22(16):2953–2958.

Raper, S. C. B. and Braithwaite, R. J. (2009). Glacier volume response time and its

links to climate and topography based on a conceptual model of glacier hypsometry. *The Cryosphere*, 3(2):183–194.

Zwally, J. (2013). Correction to the ICESat Data Product Surface Elevations due to an Error in the Range Determination from Transmit-Pulse Reference-Point Selection (Centroid vs Gaussian). Retrieved from: http://nsidc.org/data/icesat/pdf/ICESat%20G-C%20statement.pdf.